

A new method for reconstructing the 3D shape of single cells in fruit

Item Type	Journal article
Authors	Zhang, Meishuan;Yang, Jun;Wang, Yiheng;Li, Zhiguo;Tchuenbou-Magaia, Fideline Laure
Citation	Zhang, M., Yang, J., Wang, Y., Li, Z. and Tchuenbou-Magaia, F. (2022) A new method for reconstructing the 3D shape of single cells in fruit. Food Research International, 162(A), 112017.
DOI	10.1016/j.foodres.2022.112017
Publisher	Elsevier
Journal	Food Research International
Download date	2026-05-20 19:57:48
License	https://creativecommons.org/licenses/by-nc-nd/4.0/
Link to Item	http://hdl.handle.net/2436/624952

A new method for reconstructing the 3D shape of single cells in fruit

Meishuan Zhang^{a,c}, Jun Yang^{a,c}, Yiheng Wang^{a,c}, Zhiguo Li^{a,c,*}, Fideline Tchuenbou-Magaia^b

^aCollege of Mechanical and Electronic Engineering, Northwest A&F University, Yangling, 712100, China

^bSchool of Engineering, Computing and Mathematical Sciences, Division of Chemical Engineering, University of Wolverhampton, Wolverhampton, WV1 1LY, UK

^cKey Laboratory of Agricultural Internet of Things, Ministry of Agriculture and Rural Affairs, Yangling, 712100, China

*Correspondence Email: lizhiguo0821@163.com (Z. Li)

Abstract: Fruit cells' shape generally reflects the physiological state and quality of the fruit, and indirectly dictates its economics. In this study, a new bio-microscope including three independent and orthogonal channels of opto-electromechanical microscopic observation systems was developed to obtain the three views (e.g., front view, top view, side view) of a single fruit cell using tomato and strawberry at two ripening stages as fruit samples. The obtained three-view images were used to reconstruct the 3D real shape of a single cell based on the 3D geometrical modelling method using Solidworks CAD design software and then compared with the actual geometric size. The average relative errors for the major diameter, minor diameter 1, minor diameter 2, projection perimeter and projection area were 4.04 %, 6.25 %, 5.71 %, 1.69 % and 3.79 %, respectively. This good accuracy makes the newly developed bio-microscope together with the proposed 3D geometrical modelling method a promising 3D shape reconstruction technology for a single fruit cell to extract real and detailed cell morphology information. Furthermore, this method can find applications in other fields such as human and animal cells where soft particles' 3D shape analysis is important.

Keywords: Fruit; Single cell; 3D shape; Microscope; Reconstruction

Nomenclature		M	total magnification of an opto-electromechanical microscopic observation system
a	diagonal length of the image sensor in the electronic eyepiece, mm	M_1	magnification of the achromatic objective lens
b	diagonal length of the view-field image in the PC screen, mm	M_2	magnification of the reduction lens
C_p	projection perimeter of single cell, μm	M_3	magnification of the electronic eyepiece
C_{p1}	projection perimeter of a single cell in the top view, μm	n	refractive index of the optical medium between objective lens and single cell
C_{p2}	projection perimeter of a single cell in the front view, μm	NA	numerical aperture of the achromatic objective lens
C_{p3}	projection perimeter of a single cell in the side view, μm	N_{crack}	number of the cracked cells
d	resolution of an opto-electromechanical microscopic observation system, nm	N_{total}	total number of the isolated cells
D_1	minor diameter 1 of a cell, μm	P_c	percentage of the cracked cells in the isolated cells, %
D_2	minor diameter 2 of a cell, μm	S	surface area of a cell, μm^2
F_1	focus of the objective lens	S_p	projection area of single cell, μm^2
F_2	focus of the reduction lens	S_{p1}	projection area of a single cell in the top view, μm^2
GMD	geometric mean diameter of cell, μm	S_{p2}	projection area of a single cell in the front view, μm^2
l	an observed object	S_{p3}	projection area of a single cell in the side view, μm^2
l_1	an image of l through the achromatic objective lens	u	aperture angle of the objective lens, $^\circ$
l_2	an image of l_1 through the reduction lens	V	volume of a cell, μm^3
l_3	an image of l_2 through the electronic eyepiece on PC screen	λ	wavelength of the light, nm
L	major diameter of a cell, μm	φ	sphericity of a cell

21

22

23 **1. Introduction**

24 Fresh fruit is made up of millions of cells of different shapes and sizes arranged in close proximity (Chen
25 and Opara, 2013). Its textural properties depend entirely on the geometric morphology, textural mechanics and
26 chemical composition of the cells (Missang et al., 2011; Rosa-Martinez et al., 2021). The formation of cell
27 shape is mainly the result of the dynamic balance between the tension generated by the contraction of
28 microfibrils containing actin in the cell and the adhesion of the extracellular matrix attachment points (Ball et
29 al., 2012). Cells in the fruit have very different shapes depending upon the type of extracellular matrix
30 component used for cell attachment (Bronner, 2012). Cells' shape plays a leading role in the regulation of cell
31 differentiation, gene expression and tissue morphogenesis. It contains the management information of cells
32 and is an intuitive expression of cell growth and development (Prasad and Alizadeh, 2019). Understanding cell
33 shape enables inferences about the physiological conditions within the fruit life and the underlying quality
34 characteristics. As a result, it is of significant scientific value to explore the real three-dimensional (3D)
35 geometric morphological characteristics of the cells in fruit.

36 Previous literature on the observation of fruit cell morphology can be divided into two categories. One
37 focuses on the use of a biological microscope to obtain two-dimensional (2D) morphological information of
38 tissue cells in a certain view. Nieto et al. (2004) observed the microstructural and ultrastructural changes in
39 apple pulp tissues during osmotic dehydration using a biomicroscope and environmental electron scanning
40 microscope, and found that the shape of cells in fresh tissues was generally regular of equal diameter and
41 loosely arranged. McAtee et al. (2009) observed the single cells isolated from apple pulp tissue by using 0.05
42 M Na₂CO₃ solution to dissolve pectin in the middle layer of the plant cell wall, and found that their single cell
43 shape was nearly round, with different cell sizes within each variety and an average diameter of about 250
44 μm. Legland et al. (2012) used the confocal laser scanning microscope to observe tomato cells and found that
45 the mesocarp cells near the stalk were small and round, relatively uniform in size, with smaller cells in the
46 exocarp, while cells in the equatorial region were larger and longer and uneven in size. Poles et al. (2020) used
47 both optical microscope and X-ray computed micro-tomography (micro-CT) to observe apple pulp cell
48 morphology and the intercellular space, respectively. Zdunek and Kurenda (2013) used a biological
49 microscope in combination with an atomic force microscope to investigate the nano-mechanical properties
50 with topography imaging of tomato cells, and most pericarp cells in tomatoes were oval-shaped. The other
51 category of research focused on 3D morphological observations of fruit tissue cells. Angeles et al. (2004)
52 observed the morphology of the sclereid cell in pear mesocarp by confocal laser scanning microscope and

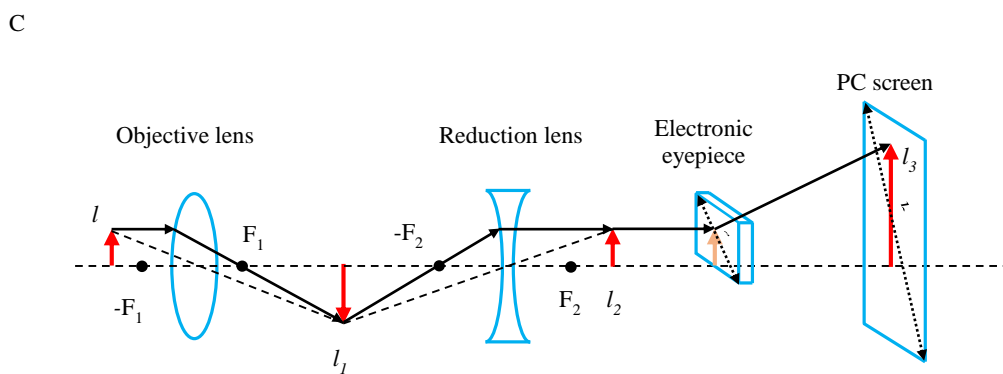
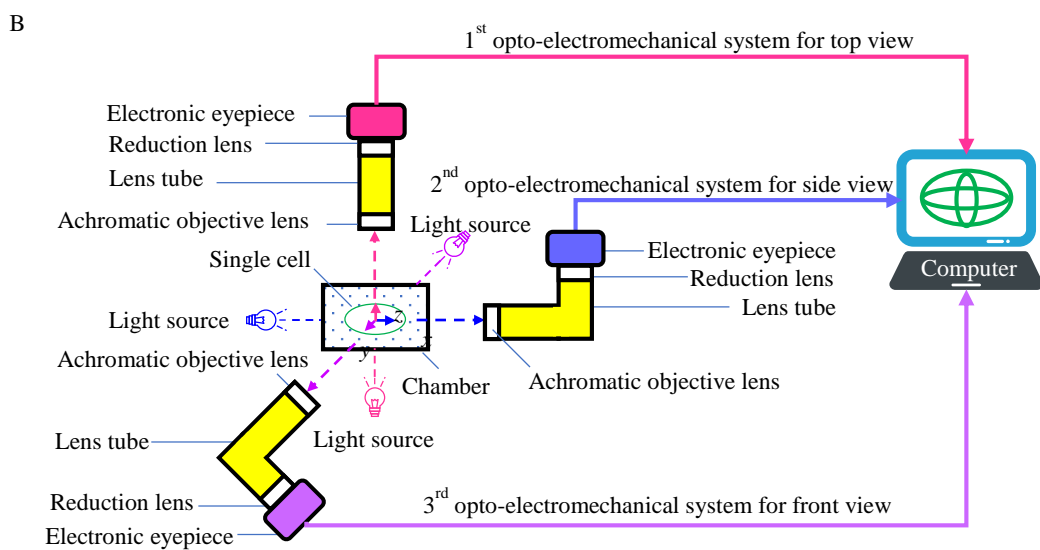
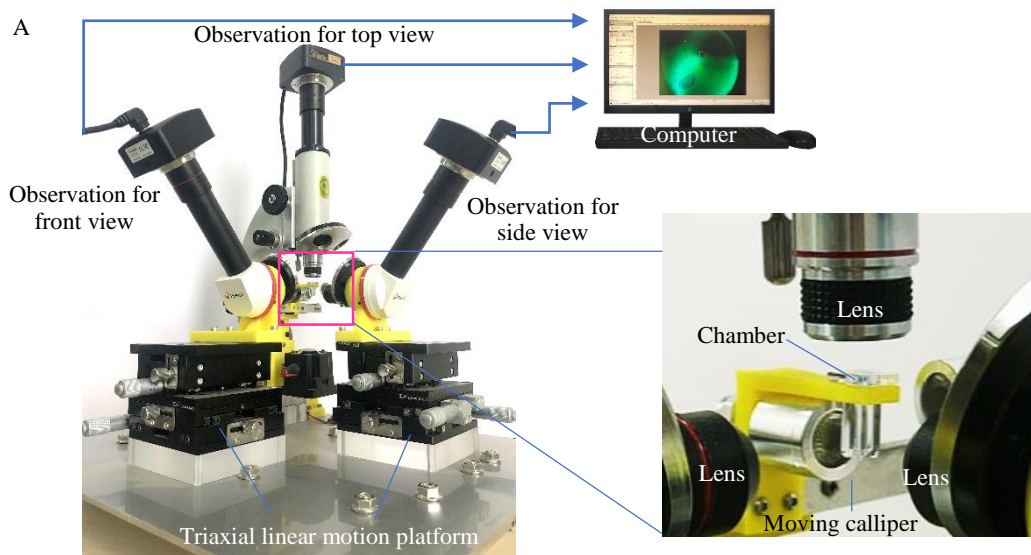
53 found that each surface of this cell contained many irregular cell walls, not in the same plane and that the pits
54 on each surface were circular. Mebatsion et al. (2009) observed the cortical tissue cells of pear and apple by
55 X-ray micro-CT technique and transmission electron microscope and reported cell wall thicknesses of $1.67 \pm$
56 $0.71 \mu\text{m}$ and $0.77 \pm 0.51 \mu\text{m}$ and mean volumes of $6.39 \pm 7.76 \times 10^5 \mu\text{m}^3$ and $2.42 \pm 3.18 \times 10^5 \mu\text{m}^3$ in apple
57 and pear, respectively. Legland et al. (2010) used the confocal laser scanning microscope to obtain 3D images
58 of tomato pericarp tissue cells and found that tomato pericarp cells exhibited different morphologies, with cells
59 close to the exocarp being smaller and aligned parallel to the epidermis, while cells away from the exocarp
60 were larger and aligned in a radial direction. Wang et al. (2018) scanned the apple peel samples continuously
61 by micro-CT and showed that the dehydration resulted in cell shrinkage, mechanical deformation and reduction
62 in cell volume throughout the tissue samples. Liu et al. (2020) studied the 3D shapes of cells in different tissues
63 of tomato fruit based on two microscopic orthogonal images, and the results showed that the fruit mesocarp
64 cells approximated ellipsoid shapes whereas the fruit endocarp cells approximated flat thin slices with serrated
65 edges.

66 Combining the above literature, many studies have been done on 2D and 3D morphology data of fruit
67 tissue cells with some limitations. For example, cells' 2D surface morphology features containing partial depth
68 information observed by environmental scanning microscope or confocal laser scanning microscope (Wood et
69 al., 2013; Zhang et al., 2022), and a partial 3D geometric information of cells in fruit tissue gained by micro-
70 CT technology (Herremans et al., 2015). However, there is little information about the 3D reconstruction of
71 single cells isolated from a fruit tissue. Although the micro-CT technology is widely used to observe the
72 microstructure of fruit tissue, its observation is based on a small block of a tissue sample. The potential hiding
73 part between cells makes this method not appropriate for obtaining the whole 3D morphological information
74 of a single cell. In addition, the accurate characterization of single-cell mechanics always requires a real single-
75 cell shape (Dintwa et al., 2011; Li et al., 2016; Wang et al., 2004). According to Hertz contact theory, the radii
76 of the curvature of two objects determines their force-displacement change law in the process of mutual contact
77 action of the two objects (Li et al., 2017). If the estimated single-cell shape deviates significantly from the real
78 cell shape (Wood et al., 2013), the single-cell mechanics characterized by Hertz contact theory will be
79 inaccurate. As a result, the goal of this study is to propose a method for reconstructing the 3D shape of single
80 cell in fruit so that a more real 3D morphology information of the fruit cells can be obtained and understood.

81 **2. Materials and methods**

82 *2.1 Development of a 3D bio-microscope*

83 Obtaining the front view, top view and side view of a single cell in fruit is the necessary condition for
84 subsequent reconstruction of the 3D shape of a single cell. Therefore, a new bio-microscope (Fig. 1A)
85 developed in our plant mechanics laboratory is presented in this study. It is mainly composed of three
86 independent and orthogonal opto-electromechanical microscopic observation systems (Fig. 1B). This bio-
87 microscope allows the shape profile information of a single cell to be observed along the x , y , and z axes of the
88 xyz Cartesian coordinate system for obtaining its front view, side view and top view, respectively (Fig. 1B).
89 The opto-electromechanical microscopic system for observing the shape profile information of the cell from
90 the front view or side view direction mainly includes: an electronic eyepiece including a 1/2.5 inch CMOS
91 image sensor with a resolution of 5 million pixels (MC - D500U/TP, Phoenix Optical Co., Ltd., China), a
92 coated reduction lens with a magnification of 0.5X (RH - 0.5X, Nanjing Nanpai Technology Co., Ltd., China),
93 a lens tube, a nosepiece, an achromatic objective lens with a magnification of 4X (Jiangxi Phoenix Optical Co.,
94 Ltd., China), a triaxial linear micro-motion platform with an accuracy of 0.03 mm (LD90 - RM-2, Shenzhen
95 Huike Pneumatic Precision Machinery Co., Ltd., China), a LED light source with a power of 0.5 W (Shitong
96 - 1500, Shenzhen Jialetu Technology Co., Ltd., China). The opto-electromechanical microscope system for
97 observing the shape profile information of the cell from the top view direction mainly includes: an electronic
98 eyepiece including a 1/2.5 inch CMOS image sensor with a resolution of 5 million pixels, a coated reduction
99 lens with a magnification of 0.5X, a lens tube, a nosepiece, a focus adjustment mechanism (coarse focus range:
100 0 - 50 mm, fine focusing range: 1.8 - 2.2 mm), an achromatic objective lens with a magnification of 4X (XSP
101 - 30, Jiangxi Phoenix Optical Co., Ltd., China), an adjustable light source with a power of 0.5 W (Phenix - 00,
102 Jiangxi Phoenix Optical Technology Co., Ltd., China). The triaxial linear micro-motion platforms in the front-
103 view and side-view opto-electromechanical microscope systems are mainly used to adjust the field position of
104 objective lens view and the distance between the objective lens and the cell sample. The stage of the bio-
105 microscope is composed of a transparent cuboid glass chamber (length \times width \times height: 5 mm \times 5 mm \times 13
106 mm, wall thickness: 1 mm), a holder and a xy axis moving calliper (vertical adjustment range: 0 - 25 mm,
107 lateral adjustment range: 0 - 50 mm, accuracy: 0.1 mm). The glass chamber is mainly used to store buffers and
108 single living cells during the observation experiment, and the moving calliper is used to adjust the position of
109 glass chamber relative to the objective lens in the opto-electromechanical microscope system for positioning
110 the top view of the single cell sample in a reasonable view field.



111

112 **Fig. 1** Structure and working principle of the self-developed bio-microscope. (A) physical structure of the bio-
 113 microscope, (B) working principle of the bio-microscope, (C) imaging principle of an opto-electromechanical
 114 system.

115 The imaging principle of each opto-electromechanical observation system of this microscope is shown in
 116 Fig.1C. The enlarged image l_1 was formed through the objective lens by an object l and the reduced image l_2

117 was formed through the reduction lens by the object l_1 and, finally, an enlarged digital image l_3 on the PC
118 screen was formed through the electronic eyepiece. Thus, the total magnification (M) of each observation
119 system was calculated by Eq. (1). The resolution of the bio-microscope (d) is used to indicate the resolving
120 power of the microscope, namely the smallest unit that the microscope can resolve, and was calculated by Eq.
121 (2).

$$122 \quad M = M_1 \cdot M_2 \cdot M_3 = M_1 \cdot M_2 \cdot \frac{b}{a} \quad (1)$$

$$123 \quad d = \frac{0.61\lambda}{NA} = \frac{1.22\lambda}{n \cdot \sin u} \quad (2)$$

124 2.2 Isolation and reconstruction of 3D single cell in a fruit

125 2.2.1 Isolation of single cells in fruit

126 40 tomato fruit (2 varieties \times 2 ripening stages \times 10 samples) and 40 strawberry fruit (2 varieties \times 2
127 ripening stages \times 10 samples) were hand-picked in the greenhouse of a family farm in Yangling Agricultural
128 High-tech Industrial Demonstration Zone, China in March 2022. Two tomato varieties were ‘Provence’ and
129 ‘Super taro’, and their two ripening stages referred to the pink (30 ~ 60 % area of fruit surface is pink or red)
130 and red (more than 90% of the fruit surface is pink or red) recognized by the reference of USDA (1991). The
131 strawberry varieties were ‘Benihoppe’ and ‘Akihiime’, with two ripening stages recognized by the reference
132 of Rahman et al. (2016): 2/3rd maturity (the surface of the fruit turns from pink to red) and full maturity (80%
133 of the fruit surface area is deep red). When picking the same variety and ripening stage of fruit, the choosing
134 standards were fruits of similar shape and size, and free of pests and diseases. Finally, these fruit samples were
135 transported into the Plant Mechanics Research Group laboratory immediately within 1 hour and kept at room
136 temperature (22 ± 1 °C, 50 ~ 55 % RH) for 30 min before the test. Because the mesocarp of tomato fruit and
137 the cortex of strawberry fruit are the main part of the fruit flesh, the two tissues were used for isolating single
138 cells for the following study.

139 Taking the isolation of mesocarp cells in tomato fruit as an example, the steps were as follows. Firstly,
140 10 ml of purified water and 3 ml of 0.5 % aqueous methylene blue solution were dropped into a 50 ml glass
141 beaker, and a tomato fruit was cut into two halves along its longitudinal equatorial section using a sharp blade.
142 Subsequently, a cuboid sample of mesocarp tissue (length \times width \times thickness: 15 mm \times 7 mm \times 3 mm) was
143 cut down from the right half of the fruit by the homemade double-blade cutter. The surface of tomato mesocarp
144 sample was gently brushed using a woollen test tube brush with 20 mm diameter and some single cells were
145 isolated from the mesocarp sample and then transferred to the solution prepared in the glass beaker. Then the
146 single cells attached to the test tube brush were rinsed into the beaker with 6 ml purified water sucked by the

147 pipette. The solution containing the single tomato cells was stirred well by a 4 mm diameter glass rod, and
148 then 3 ml of this solution containing single cells were transferred onto the slide using a 3 ml pipette. The slide
149 was then placed on the stage of a stereo microscope (XTL-165-MT, Phoenix Optical Co., Ltd., China), and the
150 magnification and focal length of the microscope were adjusted to clearly observe the single cells in the
151 solution. Only some single cells with intact morphology were selected with the help of the stereo microscope.
152 The cell which were too close to each other were dispersed as much as possible from other cells by the air
153 blown from the pipette, and using a dissecting needle if required (Li et al., 2016). Subsequently, the single cell
154 selected from the slide with a little solution around the cell was sucked into the pipette and then transferred to
155 a glass chamber with a 3 mm depth of purified water. The glass chamber was placed on the holder and secured
156 to the stage of the new bio-microscope, and the front view, top view and side view of the single cell were
157 synchronous transmitted into a Phenix software (Version: 3.0, Phoenix Optical Co., Ltd., China) of the
158 computer in real-time. Finally, the front view, top view and side view of the single cell were captured by
159 choosing different electron eyepiece channels in the software, respectively. Using similar method, totally 80
160 single tomato cells (2 varieties \times 2 ripening stages \times 20 samples) and 80 single strawberry cells (2 varieties \times
161 2 ripening stages \times 20 samples) were isolated and then observed one by one.

162 The images of 1 mm line segments on a standard calibration slide was obtained by Phenix software as a
163 measuring scale, and then the 3D size of single cells isolated from the tomato and strawberry fruit was
164 measured by a Digimizer image analysis software (Version: 5.4.4, Beijing Huanzhong Ruichi Technology Co.,
165 Ltd., China). Firstly, the longest diameter in the three views of the single cell was regarded as the major
166 diameter of single cell, and the diameter on equatorial section which was vertical to the major diameter on the
167 same image was considered as the minor diameter 1 of the single cell. Subsequently, the diameter which was
168 vertical to the major diameter and the minor diameter 1 was regarded as the minor diameter 2 of the single cell.
169 Finally, the geometric mean diameter of the single cell was calculated by Eq. (3) (An et al., 2020). The
170 sphericity of the cell which indicates the degree of deviation of the cell morphology from the standard sphere
171 was calculated by Eq. (4) (Han et al., 2022), and its surface area and volume were estimated by Eq. (5) and Eq.
172 (6), respectively (Singh et al., 2019).

173 In order to investigate the effect of fruit type, variety, ripening stage on the mechanical isolability of a
174 single cell based on the above operation method, the numbers of the cracked and total cells were counted after
175 single cells of tomato mesocarp and strawberry cortex were mechanically isolated. The methodology for single
176 cells isolated from tomato mesocarp is described here as an example. Firstly, a cuboid tissue sample (length \times

177 width × thickness: 15 mm × 7 mm × 3 mm) was cut down from tomato mesocarp by a home-made double-
 178 blade cutter. A small beaker containing 10 ml of purified water and 3 ml of 0.5 % methylene blue aqueous
 179 solution was placed below the tissue sample, and the largest surface of the sample was gently brushed 20 times
 180 by a woollen test tube brush with a diameter of 20 mm. This brushing process allows some isolated single cells
 181 to fall into the beaker. Subsequently, some purified water drops were dropped onto the test tube brush for
 182 rinsing the single cells attached to the brush into the beaker using a pipette. The solution containing isolated
 183 single cells was stirred for 5 s using a glass rod with a diameter of 4 mm, and then 5 ml solution was transferred
 184 onto the slide by the pipette. Finally, the slide was placed on the movable stage of the optical bio-microscope
 185 (PH100-3A41L-A, Phoenix Optical Co., Ltd., China). The optical bio-microscope was connected to the
 186 computer through the electronic eyepiece and the magnification and focal length of the optical bio-microscope
 187 was adjusted for observing the clear images of isolated single cells in solution. The solution containing single
 188 cells on the slide was scanned line by line by moving the movable stage of the bio-microscope. Images were
 189 captured when a single cell appeared in the view field of the bio-microscope. After the solution containing
 190 single cells on the slide was scanned completely, the images of all single cells on the slide were saved, and
 191 then the numbers of the cracked and total cells were counted. The crack rate of single cells isolated using the
 192 above method was calculated by Eq. (7). Furthermore, single cells in strawberry cortex were isolated by the
 193 same method to count the number of the cracked and total cells.

$$194 \quad GMD = (LD_1D_2)^{1/3} \quad (3)$$

$$195 \quad \varphi = \frac{GMD}{L} \quad (4)$$

$$196 \quad S = \pi(LD_1D_2)^{2/3} \quad (5)$$

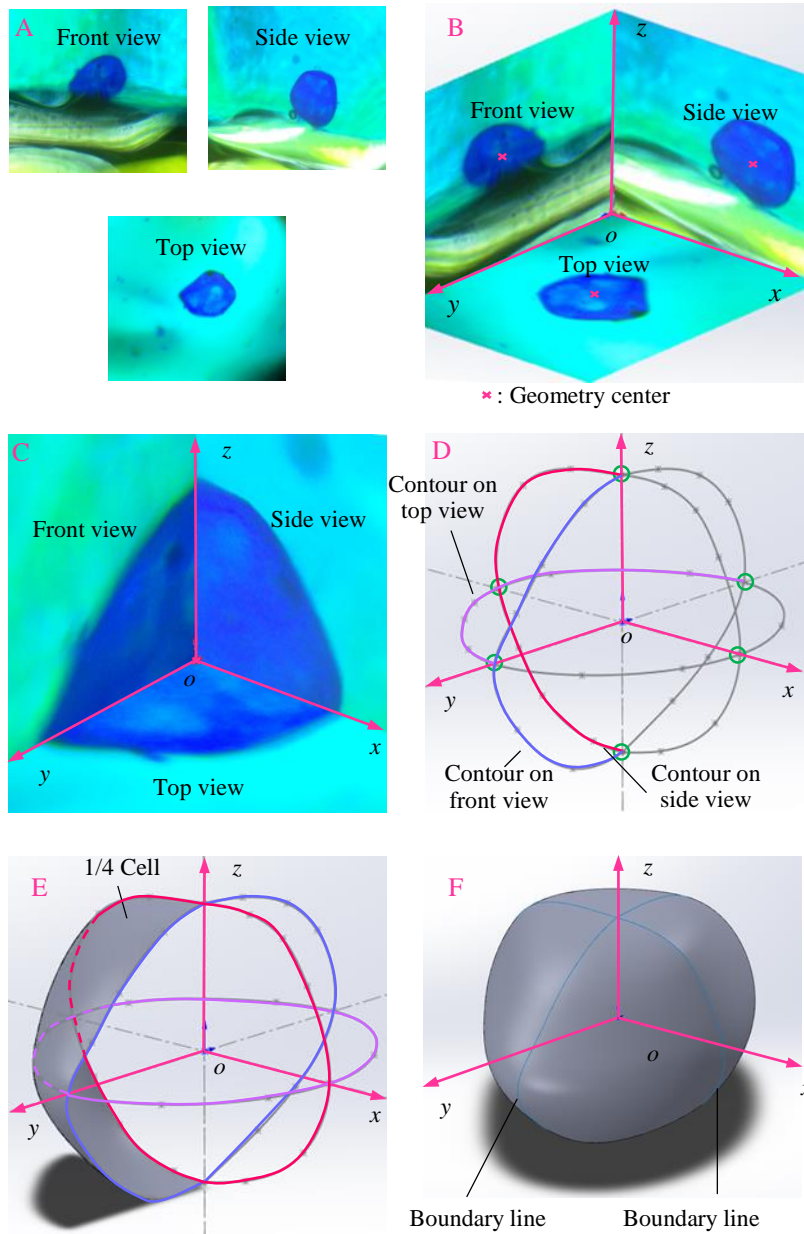
$$197 \quad V = \frac{4}{3}\pi\left(\frac{L}{2}\right)\left(\frac{D_1}{2}\right)\left(\frac{D_2}{2}\right) \quad (6)$$

$$198 \quad P_c = \frac{N_{\text{crack}}}{N_{\text{total}}} \times 100 \% \quad (7)$$

199 2.2.2 3D reconstruction of single cells in a fruit

200 From the perspective of engineering cartography, any 3D object in space has its corresponding three
 201 views: front view, side view and top view, which can be used to reconstruct the unique 3D geometry. Therefore,
 202 the idea of this study was to obtain the three views of a single cell using the self-developed bio-microscope
 203 and then reversely reconstruct the 3D shape of the single cell by the SolidWorks CAD design software (Version:
 204 2019, Dassault Systemes SOLIDWORKS Corp., France) (Fig. 2). The specific operation method was as
 205 follows: (1) After a single cell was isolated using the experimental method described in section 2.2.1, the 2D

206 front, side and top view images of the single cell in the x , y and z directions were obtained through three
207 independent and orthogonal opto-electromechanical microscope systems of the new developed bio-microscope,
208 respectively; and then these images were saved to the computer by the Phenix imaging processing software
209 (Fig. 2A). (2) The three views of the single cell were processed separately to obtain the geometric centre of
210 the single cell in each view using a Digimizer image analysis software and by adjusting the front view, side
211 view and top view of a single cell in three directions to place it in the three corresponding reference planes
212 (e.g., front plane, right plane, top plane) of the drawing space of SolidWorks software (Fig. 2B). This required
213 the three view images of the single cell to be perpendicular to each other and the geometric centre of the cell
214 was repeated to the origin of the Cartesian coordinate system in the software drawing space (Fig. 2C). (3) The
215 contour of the single cell on each view was sketched accurately by some operation commands, such as sketch
216 drawing and spline. To facilitate the following lofted surface operation, at each time only a half of the single
217 cell contour line was sketched. Some control points on each sketched contour spline curve of the single cell
218 were fine adjusted to ensure that there were two common intersections on the z axis for the front and side
219 contour lines of single cell, two common intersections on the y axis for the front and top contour lines of single
220 cell, and two common intersections on the x axis for the top and side contour lines of single cell (Fig. 2D). (4)
221 The contour lines of the single cell on the front view and side view were defined as the boundary lines whereas
222 the top view contour line was defined as the guide line, and a 1/4 single cell surface was reconstructed each
223 time using the operation command of lofted surface. In total, the whole surface of a single cell was fully created
224 by four times' similar reconstruction operations as aforementioned . Subsequently, the operation command of
225 the constraint tangency to face was used to ensure that the transitions at the adjacent junctions of four 1/4
226 surfaces of a single cell were smooth (Fig. 2E). (5) The 3D geometric solid of the single cell was finally
227 generated using knit surface and merge entities functions (Fig. 2F).



228

229 **Fig. 2** 3D reconstruction process of a single cell. (A) three views of a single cell, (B) obtaining the geometric
 230 center of each cell view, (C) placing three geometric centers together, (D) sketching the contour line of each
 231 cell view, (E) reconstructing the 1/4 cell surface, (F) generating the 3D geometric model of the single cell.

232 *2.2.3 Validation of the method for reconstructing the 3D shape of single cell*

233 In order to validate the accuracy of the above proposed 3D reconstruction method of a single cell, some
 234 geometric parameters of eight real single cells were compared to that of their corresponding 3D reconstructed
 235 cell models. Because the geometric size of cells is very small, five geometric parameters (e.g., major diameter,
 236 minor diameter 1 and 2, projection perimeter and projection area), which are easily measured by the existing
 237 commercial microscopes, were selected for this validation. The projection perimeter referred to the average
 238 value of the projection perimeters of the single cell in the three views and was calculated by Eq. (8), the

239 projection area referred to the average value of the projection areas of the single cell in the three views and
240 was calculated by Eq. (9).

$$241 \quad C_p = \frac{(C_{p1} + C_{p2} + C_{p3})}{3} \quad (8)$$

$$242 \quad S_p = \frac{(S_{p1} + S_{p2} + S_{p3})}{3} \quad (9)$$

243 *The measurement of the geometric parameters of real single cells:* eight single cells (2 fruit types \times 2
244 varieties \times 2 ripening stages) were selected from the tomato and strawberry single cells isolated in Section
245 2.2.1. Subsequently, five geometric parameters (e.g., major diameter, minor diameter 1 and 2, projection
246 perimeter and projection area) of the selected single cells were measured by the Digimizer image analysis
247 software.

248 *The measurement of the geometric parameters of 3D reconstructed model:* eight selected single fruit cells
249 were 3D reconstructed by the method in described in Section 2.2.2. Subsequently, the three views of each
250 3D reconstructed cell model were generated by the SolidWorks CAD software, and imported into the
251 Digimizer image analysis software for the measurement of five geometric parameters (e.g., major diameter,
252 minor diameter 1 and 2, projection perimeter and projection area). Finally, the geometric parameters of the
253 eight 3D reconstructed cell models were measured and recorded.

254 **3. Results and discussion**

255 *3.1 Geometric size of isolated single cells in tomato and strawberry fruit*

256 Table 1 lists the geometric parameters of fruit tissue cells isolated at different ripening stages with the
257 method of brushing the surface of the fruit tissue by the test tube brush. The results showed that this mechanical
258 isolation method can be used to isolate cells from ‘Provence’ and ‘Super taro’ tomato mesocarp tissue with the
259 geometric mean diameter, sphericity, surface area and volume of 259 ~ 333 μm , 0.74 ~ 0.84, $2.1 \times 10^5 \sim 3.7$
260 $\times 10^5 \mu\text{m}^2$, $9.2 \times 10^6 \sim 2.3 \times 10^7 \mu\text{m}^3$, respectively. The same method was proved appropriate for isolating
261 cells from ‘Benihoppe’ and ‘Akihiime’ strawberry cortex tissue with the geometric mean diameter, sphericity,
262 surface area and volume of 167 ~ 259 μm , 0.73 ~ 0.75, $9.3 \times 10^4 \sim 2.2 \times 10^5 \mu\text{m}^2$, $2.9 \times 10^6 \sim 9.7 \times 10^6 \mu\text{m}^3$,
263 respectively. The geometric mean diameter, sphericity, surface area and volume of fruit single cells were
264 significantly different between tomato and strawberry ($p < 0.05$), and the geometric mean diameter, surface
265 area and volume of mesocarp cells from tomato fruit were larger than those of cortex cells from strawberry
266 fruit. The expansion of tomato fruit cells begins after fruit setting, accompanied by cell division which lasts
267 for 1 ~ 2 weeks. This phase is followed by the second stage of cell expansion with no cells division and
268 continues throughout the fruit growth period (Azzi et al., 2015), and then the volume of a single cell in the

269 mesocarp tissue of the tomato fruit could increase by about 30000 times compared to the initial cell volume.
270 On other hand, the maximum cell diameter could be increased to 0.5 mm at the end of the second stage in cell-
271 expansion, which is mainly due to the dramatic increase in the vacuolar volume and vacuolation index of fruit
272 cells (Bourdon et al., 2010). By contrast, the strawberry fruit cells are generally dominated by cell division
273 within 10 days after anthesis while the cell expansion dominated fruit growth within the following 10 to 20
274 days by water uptake (Merlaen et al., 2018) whereas the cell division continues throughout the ripening period
275 of strawberry fruit growth (Chevalier et al., 2011). The increasing of the size and mass of strawberry fruit was
276 mainly the result of strawberry cells expansion, and cells division only accounted for 15 ~ 20 % of the total
277 fruit growth. Moreover, the average volume of strawberry cortex cells at 30 days after flowering was 0.006
278 mm³, which was 12 times larger than that at 5 days after flowering (Vallarino et al., 2018).

279 The size of fruit cells mainly depends on the gene and the growth environment of the plant. Tomato
280 belongs to the Solanum genus in the Solanaceae family, and strawberry belongs to the Fragaria genus in the
281 Rosaceae family. Because the two fruits belong to different families and genera, there are large differences
282 in gene composition and physiological regulation between tomato and strawberry (Gaston et al., 2020). The
283 growth of cell is controlled by multiple gene networks at the subcellular scale, and the cell size is closely
284 correlated with the number of endoreduplication cycles in tomato fruit and cell cycle regulation, which
285 indicates that cell size is tied to endoreduplication or cell division (Fanwoua et al., 2013). For tomato fruit, the
286 CDKA1 induced mitosis across the pericarp and altered the endoreduplication index, and its overexpression
287 indirectly affected pericarp cell expansion (Azzi et al., 2015). It was found that transgenic tomato plants
288 where the WEE1 gene has been suppressed produced smaller fruit and smaller cells in fruit tissue (Gonzalez
289 et al., 2007). Furthermore the overexpression of the SICCS52A gene accelerated endo-reduplication after
290 tomato anthesis and up to 3 days, resulting in an increase in pericarp cell size (Mathieu-Rivet et al., 2010). For
291 strawberry fruit, the expression of FaGID1c receptor reached its highest level in the white receptacle, and the
292 gibberellin is likely to be involved directly in the development of the receptacle by promoting cell expansion
293 mainly during the white stage (Csukasi et al., 2011). Zhou et al. (2021) found that the FveRGA1 gene is a
294 key regulator of fruit set and can repress the expression of cells division and expansion whereas the
295 overexpression of FaGAST2 promotes a reduction in the transgenic fruit size and plant development probably
296 through the reduction in cell size (Moyano-Canete et al., 2013).

297 Plant growth occurs through concerted water uptake and irreversible cell wall expansion. Cell size and
298 shape are controlled by the mechanism governing cells expansion which determines the morphology of tissues

299 and organs. (Li et al., 2014). Pattison et al. (2013) found that seeds are a source of auxin that diffuses, or is
 300 transported to other fruit tissues where it promotes growth by cell division and expansion. In many fleshy fruit
 301 including tomato, the sugar input into the cells in the form of sucrose is converted to glucose and fructose by
 302 invertase, or fructose and UDP glucose by sucrose synthase (Massot et al., 2010), and the accumulation of
 303 carbohydrates and sucrose in the fruit cell leads to a gradient of osmotic pressure. This pressure gradient then
 304 resulted in an increased diffusion of water, notably via aquaporins, and subsequently cell expansion, which
 305 relies on cell wall plasticity, determined partly by the activity of enzymes related to the synthesis or degradation
 306 of cell wall components in the epidermis as well as in the pericarp (Prudent et al., 2010).

307 **Table 1** Geometric parameters of the isolated cells in tomato and strawberry fruit at different ripening stages.

Geometric parameters	Tomato fruit cells				Strawberry fruit cells			
	‘Provence’ variety		‘Super taro’ variety		‘Benihoppe’ variety		‘Akihiime’ variety	
	Pink	Red	Pink	Red	2/3rd maturity	Full maturity	2/3rd maturity	Full maturity
$L, \mu\text{m}$	313 ± 49	477 ± 87	354 ± 71	343 ± 68	223 ± 51	305 ± 65	254 ± 58	362 ± 69
$D_1, \mu\text{m}$	259 ± 34	336 ± 94	295 ± 43	247 ± 51	168 ± 48	227 ± 50	180 ± 31	265 ± 54
$D_2, \mu\text{m}$	208 ± 40	248 ± 80	241 ± 44	200 ± 32	127 ± 37	166 ± 51	147 ± 29	187 ± 40
$GMD, \mu\text{m}$	255 ± 34	333 ± 79	292 ± 44	255 ± 38	167 ± 40	224 ± 49	187 ± 31	259 ± 39
ϕ	0.82 ± 0.08	0.74 ± 0.12	0.84 ± 0.09	0.76 ± 0.10	0.75 ± 0.07	0.74 ± 0.10	0.75 ± 0.11	0.73 ± 0.10
$S, \mu\text{m}^2$	(2.1 ± 0.5) $\times 10^5$	(3.7 ± 1.2) $\times 10^5$	(2.7 ± 0.8) $\times 10^5$	(2.1 ± 0.6) $\times 10^5$	(0.9 ± 0.4) $\times 10^5$	(1.6 ± 0.7) $\times 10^5$	(1.1 ± 0.3) $\times 10^5$	(2.2 ± 0.6) $\times 10^5$
$V, \mu\text{m}^3$	(9.2 ± 3.6) $\times 10^6$	(2.3 ± 1.8) $\times 10^7$	(1.4 ± 0.6) $\times 10^7$	(9.3 ± 4.1) $\times 10^6$	(2.9 ± 1.6) $\times 10^6$	(6.7 ± 5.2) $\times 10^6$	(3.7 ± 2.0) $\times 10^6$	(9.7 ± 4.2) $\times 10^6$

308 Table 2 showed the numbers of the cracked and isolated total cells from tomato and strawberry fruit.
 309 Under the same experimental conditions, the isolability of single cells from fruit was qualitatively described
 310 with the total number of isolated single cells. The total number of isolated single cells was significantly
 311 difference between two fruit types and between two ripening stages. The total number of single cells isolated
 312 from tomato mesocarp was higher than that isolated from the cortex of the strawberry. Similarly, the total
 313 number of single cells isolated from fully ripe fruit was higher when compared to less ripe fruit. These results
 314 indicate better isolability of single cells from tomato fruit and well ripe fruit when compared to strawberry
 315 fruit and less ripe fruit. As we known, the general structure of the fruit cell wall surface contains microfibrils

316 embedded in an amorphous matrix, resulting in a rigid and compact mesh-like network. The structure of the
 317 plant cell wall is composed of 3D network of polysaccharide complexes that served as a passive barrier
 318 between the interior of the cell (together with the semipermeable cell cytoplasmic membrane) and the
 319 surrounding environment (Abud et al., 2013). In order to maintain appropriate cellular hydration and bind cells
 320 together to produce fruit tissue, pectin forms a soluble, highly hydrated, and gelling fraction that is localised
 321 on the outer wall surface as well as an insoluble one connected to cellulose structure by many hydrogen bonds
 322 (Kaczkowski, 2003). Moreover, pectin is the most complex polysaccharide on the cell wall in tomato and
 323 many other fleshy fruit, which plays an important role in intercellular adhesion (Van et al., 2022). Pectin
 324 undergoes de-esterification during fruit development and ripening, and the de-esterified homogalacturonan can
 325 be cleaved by other cell wall-based enzymes, such as polygalacturonase and pectate lyase, which results in cell
 326 wall loosening and weakening of the intercellular connections (Wen et al., 2013). Hence, single cells could not
 327 be isolated from green tomato fruit tissue because the fruit tissue is not mature enough, and cells at this ripening
 328 stage are small and bound together more tightly (Blewett and Jennifer 2000). It is evident that the isolability
 329 of single cells increases with the increased degree of fruit ripening. There was no difference in the crack rate
 330 of the isolated single cells among fruit types. It may be related to the method of cell isolation used in this study.
 331 Results showed that the most suitable test material for single cell isolation by this method is the red-ripe tomato
 332 mesocarp tissue.

333 **Table 2** Number of cracked cells in tomato and strawberry fruit after isolation

Fruit type	Variety	Ripening stage	N_{total}	N_{crack}	$P_c, \%$
Tomato	Provence	Pink	98	9	9.1
		Red	114	7	6.1
	Super taro	Pink	92	9	9.7
		Red	115	11	9.5
Strawberry	Benihoppe	2/3rd maturity	51	4	7.8
		Full maturity	84	7	5.9
	Akihiime	2/3rd maturity	71	7	9.8
		Full maturity	87	8	9.1

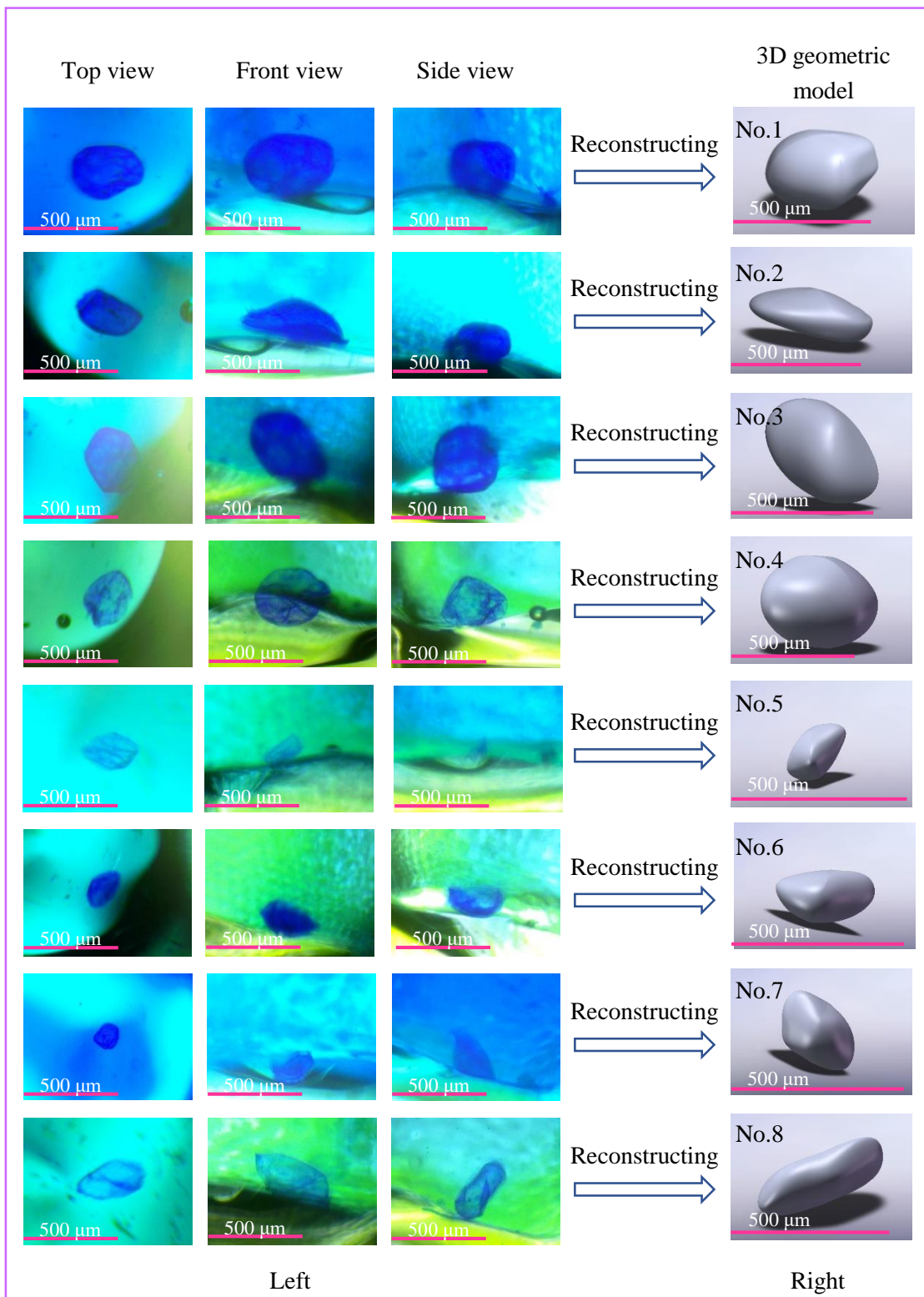
334 *3.2 Performance of the 3D single-cell reconstructing method*

335 Figure 3 shows the 3D reconstruction results of 4 tomato cells and 4 strawberry cells. In each line, the left
 336 side presented three-view images of each single cell, namely top-view image, front-view image and side-view

337 image; and the right side presented the reconstructed 3D geometric model of the corresponding single cell.
338 Obviously, the shape of single cells in fruit tissue is extremely irregular and difficult to be expressed with an
339 existing shape descriptive term. Table 3 is a comparison between the geometric parameters of real- and
340 reconstructed cells for tomato and strawberry fruit. The relative error in a geometric parameter is the percentage
341 ratio of the discrepancy between the real value (the geometric parameter value measured from a real single
342 cell) and model value (the geometric parameter value measured from its reconstructed cell model) to the real
343 value, which is used to judge the accuracy of the reconstructed 3D model of a single cell based on the above
344 proposed method in Section 2.2.2. The result showed that the average relative errors of the reconstructed single
345 cells in the major diameter, minor diameter 1, minor diameter 2, projection perimeter and projection area were
346 4.04 %, 6.25 %, 5.71 %, 1.69 % and 3.79 %, respectively. The relative error of each measured geometric
347 parameter was less than 10 %, which proved the good accuracy of the proposed reconstruction 3D model of a
348 single cell. Hence, a promising 3D shape reconstruction technology was formed by combining the newly
349 developed bio-microscope with the proposed 3D geometrical modelling method for a single fruit cell to extract
350 real and detailed cell morphology information. This method can also find applications in other fields such as
351 human and animal cell where soft particles' 3D shape analysis is important.

352 Previous studies have been done on the observation and reconstruction of 3D information at the cell scale
353 of fruit. For example, an environmental scanning microscope and a confocal laser scanning microscope were used
354 to observe 2D surface morphology characteristics of fruit tissues containing partial depth information
355 (D'Andrea et al., 2014), and the micro-CT technique was used to observe the 3D information of cells inside
356 fruit tissue (Mebatsion et al., 2010; Vicent et al., 2017; Wang et al., 2018). The working principle of the
357 confocal laser scanning microscope is that a sample is scanned point-by-point and line-by-line by the laser, and
358 the lens depth is adjusted to scan the sample layer by layer and combine the images of each layer into a 2D
359 image with the 3D feel (Amos et al., 2003). When the extraction of a fruit tissue chip is observed by this
360 method, only part of depth information on the cell surface that is not blocked can be obtained from the top
361 view, and it is difficult to obtain the fully 3D morphological information of a single cell due to different
362 overlapping cells in the tissue. Moreover, long time's laser scanning will produce the toxic light to damage the
363 tissue cells (Arora et al., 2018). For X-ray micro-CT technology an X-ray source provides the energy beam or
364 X-rays to penetrate the sample which are then captured by the X-ray detector as a 2D projection image of an
365 object in different depth based on the attenuation of the energy beam. Different X-ray projection images are
366 captured when the sample is rotated on the rotational stage by fractions of a degree. The obtained series of X-

367 ray projection images are computed into cross-sectional images which can be further processed into 3D models
368 (Zhou et al., 2018). When the micro-CT technology is used to observe a block of fruit tissue, there are always
369 some overlapping between adjacent cells in the tissue, so the 3D morphological information of a single cell
370 cannot be fully observed. In addition, a single cell is a living body and it requires a buffer solution to maintain
371 its activity during the observation. If the cell is placed in a glass chamber with buffer solution for observation
372 by micro-CT, the energy attenuation of X-ray passing through the single cell is much smaller than that through
373 the chamber, so the detector of the micro-CT equipment cannot reflect the energy attenuation law of X-ray
374 transmitted through the single cell. In this study, the proposed reconstruction method is to obtain the three
375 views of a single cell by self-developed bio-microscope and then reconstruct the 3D single cell by a CAD
376 software, which appear to be similar to the visual hull algorithm reported earlier by Laurentini (1994), Matusik
377 *et al.* (2000) and Kleinkort *et al.* (2017). It is found that the visual hull method can only reconstruct the convex
378 3D shape of an object's surface, and is not suitable for the object with concavities. For a fruit cell, its internal
379 turgor pressure generally forces the cell wall to expand outward to form a certain degree of convex cell shape.
380 Hence, the previous references also validated that the 3D single cell reconstruction method is effective. In
381 summary, the confocal laser scanning microscope and micro-CT instrument always observe the tiny tissue
382 samples while the method proposed in this paper allows the observation of living single cells one by one
383 thereby yielding a more accurate detailed information about the sample.



384

385 **Fig. 3** Reconstructed results of 4 tomato cells and 4 strawberry cells. Three images in each row of the left side
 386 shows the top view, front view and side view of each single cell while the image in each row of the right side
 387 shows the 3D reconstructed model of the corresponding single cell. No.1-4: Tomato cell, No.5-8: Strawberry
 388 cell.

389

390 **Table 3** Geometric parameters of real- and reconstructed cells for tomato and strawberry fruit.

Geometric parameters	Tomato fruit cells				Strawberry fruit cells				Average relative error, %
	Provence		Super taro		Benihoppe		Akihiime		
	Pink	Red	Pink	Red	2/3rd maturity	Full maturity	2/3rd maturity	Full maturity	
L Real value, μm	503	584	450	355	212	310	287	443	4.04 \pm
Model value, μm	482	551	470	351	205	272	279	420	1.59
Relative error, %	4.17	5.65	4.26	1.13	3.30	5.81	2.79	5.19	
D_1 Real value, μm	388	355	313	237	109	167	185	221	6.25 \pm
Model value, μm	359	344	362	262	107	179	201	239	2.49
Relative error, %	7.47	3.10	8.01	5.73	1.83	8.38	7.96	7.53	
D_2 Real value, μm	338	272	350	344	156	258	188	162	5.71 \pm
Model value, μm	333	327	362	311	145	281	194	191	2.70
Relative error, %	1.48	8.87	3.31	6.89	7.05	8.19	3.09	6.81	
C_p Real value, μm	1235	1186	1177	959	465	790	657	955	1.69 \pm
Model value, μm	1249	1232	1176	976	460	785	673	981	1.12
Relative error, %	1.09	3.76	0.08	1.74	1.15	0.67	2.38	2.62	
S_p Real value, μm^2	1.25×10^5	9.20×10^4	9.77×10^4	6.93×10^4	1.47×10^4	4.27×10^4	3.13×10^4	6.70×10^4	3.79 \pm
Model value, μm^2	1.18×10^5	9.97×10^4	1.10×10^5	7.10×10^4	1.47×10^4	4.37×10^4	3.37×10^4	6.53×10^4	2.66
Relative error, %	5.60	7.69	2.98	2.35	0.00	2.29	6.93	2.49	

391 **Note:** ‘Provence’ and ‘Super taro’ – two tomato varieties, ‘Benihoppe’ and ‘Akihiime’ - two strawberry
 392 varieties.

393 3.3 Potential source of error and mitigations

394 Table 3 highlights an average relative error range of 1.69 to 6.25% between real- and reconstructed single
 395 cell based on the proposed 3D single cell reconstruction method. Potential sources of errors could include the
 396 following. (1) There may be some errors introduced during the 3D geometric reconstructing process of the
 397 single cell. The contour line on each view of the single cell was geometric generated by splining some contour
 398 points captured manually from each view image. Because it is difficult to very accurately extract the contour
 399 points of the single cell from each view image manually, it is impossible to guarantee that the generated spline
 400 curve coincides exactly with the actual contour line of the single cell. Therefore, researchers can only extract

401 the contour points of the single cell as much as possible for ensuring that the sketched contour line coincides
402 with the actual contour line of the single cell. Furthermore, in the reconstruction process as presented in Section
403 2.2.2, in order to ensure that the three views have two common intersections on each coordinate axis, some of
404 the captured contour points on each view image need fine-tuning, so this process might introduce some errors
405 as it could slightly affect the real single fruit cell shape. (2) There may be some errors in the measurement
406 process of the geometric size of the single-cell model. After a single cell is 3D geometric reconstructed, its
407 diameter was manually measured by marking two measurement points on each view image of the 3D single
408 cell model. The selected measurement points on the cell model images may be slightly different from the
409 measurement points on the real single cell. This source of error can be reduced by ensuring that the
410 measurement point selected to measure the size of the single cell 3D model coincides with the measurement
411 point selected to measure the actual size of the single cell as much as possible. (3) The shape of the cell is very
412 complex, and there may be some tiny features on the cell surface, such as folds and particles. The proposed
413 3D single cell reconstruction method always ignores these special tiny features, and only uses some main
414 contour information of a single cell in three views. Therefore, the proposed method can reconstruct the main
415 3D morphological features of a single cell, but cannot express some more tiny features on the surface of a cell.
416 Thus there exist some differences between the 3D reconstruction cell model and the real single cell, although,
417 the level of errors is within the acceptable limit. Perhaps more directional views of a single cell can be applied
418 to this reconstruction method to improve this accuracy in the future research.

419 **4. Conclusion**

420 This study provides a method to reconstruct the 3D shape of a single cell in fruit. A newly developed bio-
421 microscope was used to extract view images of a single cell and then reconstruct the single cell with the aid of
422 the Solidworks CAD design software. This bio-microscope is made up of three independent and orthogonal
423 channels of light-mechatronic systems for obtaining the front view, top view and side view, and the software-
424 based 3D geometrical modelling technology reconstructed the 3D real shape of the single cell based on the
425 obtained three-view images. Results showed that the cells in the ripe tomato and strawberry tissues were more
426 suited to be observed for reconstruction by the newly developed 3D bio-microscope because these cells were
427 relatively easy to be mechanically isolated into non-cracked single cells. Because the single cell sample can be
428 observed from its front, top and side directions, the proposed reconstruction technology is different from the
429 existing observation methods by the confocal laser scanning microscope (partial depth information) or micro-
430 CT (X-ray computed tomography), and might show more abundant 3D shape information than the previous

431 two methods. This new method could be applied to characterise other single soft particles such as vegetables
432 and animal cells as well as other colloidal particles with broad industrial applications.

433 **CRediT authorship contribution statement**

434 **Meishuan Zhang:** Conceptualization, Methodology, Investigation, Data curation, Writing - original draft.

435 **Jun Yang:** Data curation, Writing - original draft. **Yiheng Wang:** Writing - review & editing. **Zhiguo Li** and

436 **Fideline Tchuenbou-Magaia:** Writing - review & editing, Supervision.

437 **Declaration of Competing Interest**

438 The authors declare that they have no known competing financial interests or personal relationships that
439 could have appeared to influence the work reported in this paper.

440 **Acknowledgements**

441 This work was supported by a European Marie Curie International Incoming Fellowship (326847 and
442 912847), a Chinese Universities Scientific Fund (2452018313), and an International Cooperation Key Plan
443 of Shaanxi Province (2022KWZ-12).

444 **References**

445 Abud, Y., Costa, L. T., de Souza, W., & Sant'Anna, C. (2013). Revealing the microfibrillar arrangement of
446 the cell wall surface and the macromolecular effects of thermochemical pretreatment in sugarcane by
447 atomic force microscope. *Industrial Crops and Products*, 51, 62-69.
448 <https://doi.org/10.1016/j.indcrop.2013.08.076>.

449 Amos, W. B., & White, J. G. (2003). How the confocal laser scanning microscope entered biological research.
450 *Biology of the Cell*, 95(6), 335-342. [https://doi.org/10.1016/S0248-4900\(03\)00078-9](https://doi.org/10.1016/S0248-4900(03)00078-9).

451 An, X., Li, Z., Zude-Sasse, M., Tchuenbou-Magaia, F., & Yang, Y. (2020). Characterization of textural failure
452 mechanics of strawberry fruit. *Journal of Food Engineering*, 282, Article 110016.
453 <https://doi.org/10.1016/j.jfoodeng.2020.110016>.

454 Angeles, G., Owens, S. A., & Ewers, F. W. (2004). Fluorescence shell: a novel view of sclereid morphology
455 with the confocal laser scanning microscope. *Microscope Research and Technique*, 63(5), 282-288.
456 <https://doi.org/10.1002/jemt.20043>.

457 Arora, D., Singh, N., & Bhatla, S.C. (2018). Electrophoretic detection and confocal microscopic imaging of
458 tyrosine nitrated proteins in plant tissue, In: Mengel, A., Lindermayr, C (Eds.), *Nitric Oxide* (pp. 171-
459 182). Humana Press.

- 460 Azzi, L., Deluche, C., Gévaudant, F., Frangne, N., Delmas, F., Hernould, M., & Chevalier, C. (2015). Fruit
461 growth-related genes in tomato. *Journal of Experimental Botany*, 66(4), 1075-1086.
462 <https://doi.org/10.1093/jxb/eru527>.
- 463 Ball, S. G., Shuttleworth, A., & Kielty, C. M. (2012). Inhibition of platelet-derived growth factor receptor
464 signaling regulates Oct4 and Nanog expression, cell shape, and mesenchymal stem cell potency. *Stem*
465 *Cells*, 30(3), 548-560. <https://doi.org/10.1002/stem.1015>.
- 466 Blewett, Jennifer, M., (2000). Micromanipulation of plant cell mechanical properties. the University of
467 Birmingham, Birmingham,UK, pp. 546-550.
- 468 Bourdon, M., Frangne, N., Mathieu-Rivet, E., Nafati, M., Cheniclet, C., Renaudin, J.P., Chevalier, C. (2010).
469 Endoreduplication and growth of fleshy fruit, in: U.Lüttge, W.Beyschlag, B.Büdel, & D. Francis (Eds.),
470 *Progress in Botany 71* (pp. 101-132). Springer Berlin, Heidelberg.
- 471 Bronner, F. (2012). Cell shape: determinants, regulation, and regulatory role, in: D.E.Ingber, J.Folkman (Eds.),
472 *Tention and compression as basic determinants of cell form and function: utilization of a cellular*
473 *tensegrity mechanism* (pp. 2-31). Academic Press Inc.
- 474 Chen, L., & Opara, U. L. (2013). Texture measurement approaches in fresh and processed foods - A review.
475 *Food Research International*, 51(2), 823-835. <https://doi.org/10.1016/j.foodres.2013.01.046>.
- 476 Chevalier, C., Nafati, M., Mathieu-Rivet, E., Bourdon, M., Frangne, N., Cheniclet, C., Renaudin, J.,
477 Gévaudant, F., & Hernould, M. (2011). Elucidating the functional role of endoreduplication in tomato
478 fruit development. *Annals of Botany*, 107(7), 1159-1169. <https://doi.org/10.1093/aob/mcq257>.
- 479 Csukasi, F., Osorio, S., Gutierrez, J.R., Kitamura, J., Giavalisco, P., Nakajima, M., Fernie, A.R., Rathjen, J.P.,
480 Botella, M.A., Valpuesta, V., & Medina-Escobar, N. (2011). Gibberellin biosynthesis and signalling
481 during development of the strawberry receptacle. *New Phytologist*, 191, 376-390.
482 <https://doi.org/10.1111/j.1469-8137.2011.03700.x>.
- 483 D'Andrea, L., Amenós, M., & Rodríguez-Concepción, M. (2014). Confocal laser scanning microscope
484 detection of chlorophylls and carotenoids in chloroplasts and chromoplasts of tomato fruit, in: M.
485 Rodríguez-Concepción (Eds.), *Plant Isoprenoids* (pp. 227-232). Humana Press.
- 486 Dintwa, E., Jancsó, P., Mebatsion, H.K., Verlinden, B., Verboven, P., Wang, C.X., Thomas, C.R., Tijssens,
487 E., Ramon, H., & Nicolai, B. (2011). A finite element model for mechanical deformation of single tomato
488 suspension cells. *Journal of Food Engineering*, 103(3), 265-272.
489 <https://doi.org/10.1016/j.jfoodeng.2010.10.023>.

490 Dreher, M. L. (2018). Whole fruits and fruit fiber emerging health effects. *Nutrients*, 10(12), 1833.
491 <https://doi.org/10.3390/nu10121833>.

492 Estrada-Johnson, E., Csukasi, F., Pizarro, C.M., Vallarino, J.G., Kiryakova, Y., Vioque, A., Brumos, J.,
493 Medina-Escobar, N., Botella, M.A., Alonso, J.M., Fernie, A.R., Sanchez-Sevilla, J.F., Osorio, S., &
494 Valpuesta, V. (2017). Transcriptomic analysis in strawberry fruits reveals active auxin biosynthesis and
495 signaling in the ripe receptacle. *Frontiers in Plant Science*, 8, 889.
496 <https://doi.org/10.3389/fpls.2017.00889>.

497 Fanwoua, J., Visser, P. H., Heuvelink, E., Yin, X., Struik, P. C., & Marcelis, L. F. (2013). A dynamic model
498 of tomato fruit growth integrating cell division, cell growth and endoreduplication. *Functional Plant*
499 *Biology*, 40(11), 1098-1114. <https://doi.org/10.1071/FP13007>.

500 Fulker, M. J. (2001). The role of fruit in the diet. *Journal of Environmental Radioactivity*, 52(2-3), 147-157.
501 [https://doi.org/10.1016/s0265-931x\(00\)00030-8](https://doi.org/10.1016/s0265-931x(00)00030-8).

502 Gaston, A., Osorio, S., Denoyes, B., & Rothan, C. (2020). Applying the solanaceae strategies to strawberry
503 crop improvement. *Trends in Plant Science*, 25(2), 130-140. <https://doi.org/10.1016/j.tplants.2019.10.003>.

504 Gonzalez, N., Gévaudant, F., Hernould, M., Chevalier, C., & Mouras, A. (2007). The cell cycle-associated
505 protein kinase WEE1 regulates cell size in relation to endoreduplication in developing tomato fruit. *The*
506 *Plant Journal*, 51(4), 642-655. <https://doi.org/10.1111/j.1365-313X.2007.03167.x>.

507 Han, X., An, X., Fadji, T., Li, Z., & Khojastehpour, M. (2022). Textural thermo-mechanical properties of
508 sweet cherry for postharvest damage analysis. *Journal of Texture Studies*, 53: 453-464.
509 <https://doi.org/10.1111/jtxs.12661>.

510 Herremans, E., Verboven, P., Verlinden, B. E., Cantre, D., Abera, M., Wevers, M., & Nicolai, B. M. (2015).
511 Automatic analysis of the 3-D microstructure of fruit parenchyma tissue using X-ray micro-CT explains
512 differences in aeration. *BMC Plant Biology*, 15(1), 1-14. <https://doi.org/10.1186/s12870-015-0650-y>.

513 Kączkowski, J. (2003). Structure, function and metabolism of plant cell wall. *Acta Physiologiae Plantarum*,
514 25(3), 287-305. <https://doi.org/10.1007/s11738-003-0010-7>.

515 Kleinkort, C., Huang, G. J., Bringi, V. N., & Notaroš, B. M. (2017). Visual hull method for realistic 3D particle
516 shape reconstruction based on high-resolution photographs of snowflakes in free fall from multiple views.
517 *Journal of Atmospheric and Oceanic Technology*, 34(3), 697-702. <https://doi.org/10.1175/JTECH-D-16->
518 0099.1.

519 Lamport, D. J., Saunders, C., Butler, L. T., & Spencer, J. P. (2014). Fruits, vegetables, 100% juices, and
520 cognitive function. *Nutrition Reviews*, 72(12), 774-789. <https://doi.org/10.1111/nure.12149>.

521 Laurentini, A. (1994). The visual hull concept for silhouette-based image understanding. *IEEE Transactions*
522 *on Pattern Analysis and Machine Intelligence*, 16(2), 150-162. <https://doi.org/10.1109/34.273735>.

523 Legland, D., Devaux, M. F., Bouchet, B., Guillon, F., & Lahaye, M. (2012). Cartography of cell morphology
524 in tomato pericarp at the fruit scale. *Journal of Microscopy*, 247(1), 78-93. <https://doi.org/10.1111/j.1365-2818.2012.03623.x>.

526 Legland, D., Guillon, F., Kiêu, K., Bouchet, B., & Devaux, M. F. (2009). Stereological estimation of cell wall
527 density of DR12 tomato mutant using three-dimensional confocal imaging. *Annals of botany*, 105(2),
528 265-276. <https://doi.org/10.1093/aob/mcp283>.

529 Li, Z., Miao, F., & Andrews, J. (2017). Mechanical models of compression and impact on fresh fruits.
530 *Comprehensive Reviews in Food Science and Food Safety*, 16(6), 1296-1312.
531 <https://doi.org/10.1111/1541-4337.12296>.

532 Li, Z., Zhang, Z., & Thomas, C. (2016). Viscoelastic-plastic behavior of single tomato mesocarp cells in high
533 speed compression-holding tests. *Innovative Food Science & Emerging Technologies*, 34, 44-50.
534 <https://doi.org/10.1016/j.ifset.2016.01.011>.

535 Liu, Z., Li, Z., Yue, T., Diels, E., & Yang, Y. (2020). Differences in the cell morphology and microfracture
536 behaviour of tomato fruit tissues during ripening. *Postharvest Biology and Technology*, 164, Article
537 111182. <https://doi.org/10.1016/j.postharvbio.2020.111182>.

538 Massot, C., Génard, M., Stevens, R., & Gautier, H. (2010). Fluctuations in sugar content are not determinant
539 in explaining variations in vitamin C in tomato fruit. *Plant Physiology and Biochemistry*, 48(9), 751-757.
540 <https://doi.org/10.1016/j.plaphy.2010.06.001>.

541 Matusik, W., Buehler, C., Raskar, R., Gortler, S. J., & McMillan, L. (2000). Image-based visual hulls, In J. R.
542 Brown, K. Akeley(Eds.), *Proceedings of the 27th annual conference on Computer graphics and*
543 *interactive techniques* (pp. 369-374). ACM Press.

544 Mathieu-Rivet, E., Gévaudant, F., Sicard, A., Salar, S., Do, P.T., Mouras, A., Fernie, A.R., Gibon, Y., Rothan,
545 C., & Chevalier, C. (2010). Functional analysis of the anaphase promoting complex activator CCS52A
546 highlights the crucial role of endo-reduplication for fruit growth in tomato. *The Plant Journal*, 62(5), 727-
547 741. <https://doi.org/10.1111/j.1365-313X.2010.04198.x>.

548 McAtee, P. A., Hallett, I. C., Johnston, J. W., & Schaffer, R. J. (2009). A rapid method of fruit cell isolation
549 for cell size and shape measurements. *Plant methods*, 5(1), 1-7. <https://doi.org/10.1186/1746-4811-5-5>.

550 Mebatsion, H.K., Verboven, P., Ho, Q.T., & Nicolai, B.M. (2010). 3-D virtual fruit microstructure modelling.
551 *Acta Horticulturae*, 858, 473-477. <https://doi.org/10.17660/actahortic.2010.858.72>.

552 Mebatsion, H. K., Verboven, P., Endalew, A. M., Billen, J., Ho, Q. T., & Nicolai, B. M. (2009). A novel
553 method for 3-D microstructure modeling of pome fruit tissue using synchrotron radiation tomography
554 images. *Journal of Food Engineering*, 93(2), 141-148. <https://doi.org/10.1016/j.jfoodeng.2009.01.008>.

555 Merlaen, B., De Keyser, E., & Van Labeke, M. C. (2018). Identification and substrate prediction of new
556 *Fragaria x ananassa* aquaporins and expression in different tissues and during strawberry fruit
557 development. *Horticulture Research*, 5, 20. <https://doi.org/10.1038/s41438-018-0019-0>.

558 Missang, C. E., Maingonnat, J. F., Renard, C. M., & Audergon, J. M. (2011). Texture variation in apricot:
559 Intra-fruit heterogeneity, impact of thinning and relation with the texture after cooking. *Food Research*
560 *International*, 44(1), 46-53. <https://doi.org/10.1016/j.foodres.2010.11.017>.

561 Moyano-Canete, E., Bellido, M.L., Garcia-Caparros, N., Medina-Puche, L., Amil-Ruiz, F., Gonzalez-Reyes,
562 J.A., Caballero, J.L., Munoz-Blanco, J., & Blanco-Portales, R. (2013). FaGAST2, a strawberry ripening-
563 related gene, acts together with FaGAST1 to determine cell size of the fruit receptacle. *Plant and cell*
564 *physiology*, 54(2), 218-236. <https://doi.org/10.1093/pcp/pcs167>.

565 Nieto, A. B., Salvatori, D. M., Castro, M. A., & Alzamora, S. M. (2004). Structural changes in apple tissue
566 during glucose and sucrose osmotic dehydration: shrinkage, porosity, density and microscopic features.
567 *Journal of Food Engineering*, 61(2), 269-278. [https://doi.org/10.1016/S0260-8774\(03\)00108-0](https://doi.org/10.1016/S0260-8774(03)00108-0).

568 Pattison, R. J., Csukasi, F., & Catalá, C. (2014). Mechanisms regulating auxin action during fruit development.
569 *Physiologia plantarum*, 151(1), 62-72. <https://doi.org/10.1111/ppl.12142>.

570 Payasi, A., Mishra, N. N., Chaves, A. L. S., & Singh, R. (2009). Biochemistry of fruit softening: an overview.
571 *Physiology and Molecular Biology of Plants*, 15(2), 103-113. <https://doi.org/10.1007/s12298-009-0012->
572 [z](https://doi.org/10.1007/s12298-009-0012-z).

573 Poles, L., Gentile, A., Giuffrida, A., Valentini, L., Endrizzi, I., Aprea, E., Gasperi, F., Distefano, G., Artioli,
574 G., La Malfa, S., Costa, F., Lovatti, L., & Guardo, M. (2020). Role of fruit flesh cell morphology and
575 MdPG1 allelotype in influencing juiciness and texture properties in apple. *Postharvest Biology and*
576 *Technology*, 164, Article 111161. <https://doi.org/10.1016/j.postharvbio.2020.111161>.

577 Prasad, A., & Alizadeh, E. (2019). Cell form and function: interpreting and controlling the shape of adherent
578 cells. *Trends in Biotechnology*, 37(4), 347-357. <https://doi.org/10.1016/j.tibtech.2018.09.007>.

579 Prudent, M., Bertin, N., Genard, M., Munos, S., Rolland, S., Garcia, V., Petit, J., Baldet, P., Rothan, C., &
580 Causse, M. (2010). Genotype-dependent response to carbon availability in growing tomato fruit. *Plant,*
581 *Cell & Environment*, 33(7), 1186-1204. <https://doi.org/10.1111/j.1365-3040.2010.02139.x>.

582 Rahman, M. M., Moniruzzaman, M., Ahmad, M. R., Sarker, B. C., & Alam, M. K. (2016). Maturity stages
583 affect the postharvest quality and shelf-life of fruits of strawberry genotypes growing in subtropical
584 regions. *Journal of the Saudi Society of Agricultural Sciences*, 15(1), 28-37.
585 <https://doi.org/10.1016/j.jssas.2014.05.002>.

586 Rejman, K., Górska-Warsewicz, H., Kaczorowska, J., & Laskowski, W. (2021). Nutritional significance of
587 fruit and fruit products in the average polish diet. *Nutrients*, 13(6), 2079.
588 <https://doi.org/10.3390/nu13062079>.

589 Rosa-Martínez, E., García-Martínez, M. D., Adalid-Martínez, A. M., Pereira-Dias, L., Casanova, C., Soler, E.,
590 Figas, M. R., Raigon, M. D., Plazas, M., Soler, S., & Prohens, J. (2021). Fruit composition profile of
591 pepper, tomato and eggplant varieties grown under uniform conditions. *Food Research International*, 147,
592 Article 110531. <https://doi.org/10.1016/j.foodres.2021.110531>.

593 Singh, S. S., Abdullah, S., Pradhan, R. C., & Mishra, S. (2019). Physical, chemical, textural, and thermal
594 properties of cashew apple fruit. *Journal of Food Process Engineering*, 42(5), Article e13094.
595 <https://doi.org/10.1111/jfpe.13094>.

596 United States Department of Agriculture. (1991). United states standards for grades of fresh tomatoes.
597 <https://www.ams.usda.gov/grades-standards/tomato-grades-and-standards>.

598 Vallarino, J.G., de Abreu, E.L.F., Soria, C., Tong, H., Pott, D.M., Willmitzer, L., Fernie, A.R., Nikoloski, Z.,
599 & Osorio, S. (2018). Genetic diversity of strawberry germplasm using metabolomic biomarkers. *Scientific*
600 *Reports*, 8(1), 1-13. <https://doi.org/10.1038/s41598-018-32212-9>.

601 Van, A., J., Bernaerts, T., Putri, N. I., Van Rooy, L., Van Loey, A. M., & Hendrickx, M. E. (2022). The role
602 of mechanical collapse by cryogenic ball milling on the effect of high-pressure homogenization on the
603 microstructural and texturizing properties of partially pectin-depleted tomato cell wall material. *Food*
604 *Research International*, 155, Article 111033. <https://doi.org/10.1016/j.foodres.2022.111033>.

- 605 Vicent, V., Verboven, P., Ndoye, F. T., Alvarez, G., & Nicolai, B. (2017). A new method developed to
606 characterize the 3D microstructure of frozen apple using X-ray micro-CT. *Journal of Food Engineering*,
607 212, 154-164. <https://doi.org/10.1016/j.jfoodeng.2017.05.028>.
- 608 Vincente, A.R., Manganaris, G.A., Ortiz, C.M., Sozzi, G.O., Crisosto, C.H. (2014). Nutritional quality of fruit
609 and vegetables, postharvest handling, in: W. Florkowski, R. Shewfelt, N. Banks, S. Prussia (Eds.),
610 *Postharvest Handling* (pp. 69-122.). Academic Press, New York.
- 611 Wang, C. X., Wang, L., & Thomas, C. R. (2004). Modelling the mechanical properties of single suspension-
612 cultured tomato cells. *Annals of Botany*, 93(4), 443-453. <https://doi.org/10.1093/aob/mch062>.
- 613 Wang, Z., Rogge, S., Abera, M., van Dael, M., Van Nieuwenhove, V., Verboven, P., Sijbers, J., & Nicolai, B.
614 (2018). Understanding microstructural deformation of apple tissue from 4D micro-CT imaging. *Acta*
615 *Horticulturae*, 1197, 7-14. <https://doi.org/10.17660/ActaHortic.2018.1197.2>.
- 616 Wen, B., Ström, A., Tasker, A., West, G., & Tucker, G. A. (2013). Effect of silencing the two major tomato
617 fruit pectin methylesterase isoforms on cell wall pectin metabolism. *Plant Biology*, 15(6), 1025-1032.
618 <https://doi.org/10.1111/j.1438-8677.2012.00714.x>.
- 619 Wood, S. T., Dean, B. C., & Dean, D. (2013). A linear programming approach to reconstructing subcellular
620 structures from confocal images for automated generation of representative 3D cellular models. *Medical*
621 *Image Analysis*, 17(3), 337-347. <https://doi.org/10.1016/j.media.2012.12.002>.
- 622 Zdunek, A., & Kurenda, A. (2013). Determination of the elastic properties of tomato fruit cells with an atomic
623 force microscope. *Sensors*, 13(9), 12175-12191. <https://doi.org/10.3390/s130912175>.
- 624 Zhang, M., Wang, Y., Wang, J., Li, Z., & Tchuenbou-Magaia, F. (2022). Development of a new bio-
625 microscope for 3D geometry characterization of fruit single cells. *Journal of Texture Studies*, 53, 12719.
626 <https://doi.org/10.1111/jtxs.12719>.
- 627 Zhou, J., Sittmann, J., Guo, L., Xiao, Y., Huang, X., Pulapaka, A., & Liu, Z. (2021). Gibberellin and auxin
628 signaling genes RGA1 and ARF8 repress accessory fruit initiation in diploid strawberry. *Plant Physiology*,
629 185(3), 1059-1075. <https://doi.org/10.1093/plphys/kiaa087>.
- 630 Zhou, X. P., & Xiao, N. (2018). 3D numerical reconstruction of porous sandstone using improved simulated
631 annealing algorithms. *Rock Mechanics and Rock Engineering*, 51(7), 2135-2151.
632 <https://doi.org/10.1007/s00603-018-1451-z>.

633

634